Nano-scratch testing of (Ti,Fe)N_x thin films on silicon

B.D. Beake[1,*], V.M. Vishnyakov[2] and A.J. Harris[1]

[1] *Micro Materials Ltd., Willow House, Ellice Way, Yale Business Village, Wrexham, LL13 7YL, UK*

[2] *Materials Research Institute, University of Huddersfield, Huddersfield, HD1 3DH, UK*

* Corresponding author. Email: ben@micromaterials.co.uk. Tel: +44 1978 261615.

Abstract

Thin films of (Ti,Fe)N_x have been produced on silicon wafers with a wide range of compositions and mechanical properties to investigate correlations between the mechanical properties measured by indentation and crack resistance in the highly loaded sliding contact in a nano-scratch test. The nano-scratch test data on the thin films using a well-worn Berkovich indenter with ~1 μm end radius were supported by high resolution scanning electron microscopic (SEM) imaging and analytical stress modelling. The results show that mechanical properties of the coating, its thickness and the substrate properties all influence the deformation process. They affect the critical loads required, the type of failures observed and their location relative to the moving probe. The differences in coating mechanical properties affect how the interface is weakened (i.e. by initial substrate or coating yielding or both) and determine the deformation failure mechanism. The load dependence of the friction coefficient provides details of the sliding contact zone and the location of failure relative to the sliding probe. Improved performance was achieved at intermediate hardness and H^3/E^2 in the nano-scratch tests on thin films. The friction and modelling results strongly suggest that failure at low load on the hardest coatings is due to a combination of high tensile stress at the

rear of the contact zone and substrate yield. Designing thin films for protective coatings with in-built dissipative structures (such as soft and low elastic modulus inclusions) and mechanisms to combat stress may be a more successful route to optimise their toughness in highly loaded sliding conditions than aiming to minimise plasticity by increasing their hardness.

Keywords: crack resistance, protective coatings, nano-scratch, soft inclusions, H^3/E^2

Introduction

The successful use of ceramic thin films as protective coatings in demanding applications heavily relies on understanding their properties and the ability to predict their behaviour based on other more easily measured properties. With the popularity of Archard's law, hardness has long been considered the most important property for wear resistant materials. However, it has gradually been realised that other parameters combining hardness (H) and elastic modulus (E), such as H/E and H^3/E^2 may be equally important predictors of wear in many practical applications. In dry sliding and abrasive contact wear resistance has been found to correlate more closely with H/E than with hardness alone [1-2]. The dimensionless ratio H/E is a measure of the elastic strain to break and is strongly correlated with energy dissipation in mechanical contact and can easily be obtained in a nanoindentation test from H/E_r (where E_r is the reduced indentation modulus) [4-7]. In a nanoindentation test the parameter H/E_r is correlated (i) with the indentation plasticity index which is the plastic or irreversible work done during indentation (W_p) divided by the total elastic (W_e) and plastic work done during the indentation and (ii) with h_r/h_{max} where h_r = residual indentation depth and h_{max} = maximum indentation depth with the relationship taking the form

$$Plasticity\ index = W_p/(W_p + W_e) \approx h_r/h_{max} \approx 1 - x(H/E_r) \qquad [1]$$

The reduced indentation modulus E_r appears in Eqn. 1 rather than the elastic modulus since the shape of the indentation curve is subtly influenced by the stiffness of the indenter, so that lower plasticity indices and greater elastic recovery are observed with lower modulus cBN and sapphire indenters than with diamond [8]. H^3/E^2 is a measure of the resistance to plastic deformation. According to the contact mechanics analysis developed by Johnson, the critical load for the onset of plastic flow should scale with H^3/E^2 in the spherical indentation of bulk materials [9] so for a given applied load contact is more likely to be elastic if H^3/E^2 is increased.

Increasing hardness is often associated with a reduction in toughness, and high hardness alone is no guarantee of high wear resistance in highly loaded mechanical or tribological contact applications where toughness and damage tolerance can be more critical. Ceramic thin-film research has moved away from focusing solely on hardness towards developing hard-yet-tough or super-tough coatings that are designed to be crack resistant and damage tolerant under severe contact conditions [10-23]. Toughening strategies include ductile phase toughening (for example by addition of metallic phases such as Al to hard amorphous carbon films, or Ni to nc-MeN/a-SiN_x), compressive stress toughening, mechanical property optimization combined with optimization of the coating architecture by developing coatings with dense non-columnar microstructures, gradient structures with no stress discontinuities from sharp interfaces or multilayered structures with a high number of interfaces for crack deflection. In highly loaded contact applications, coatings with higher plasticity in indentation (i.e. lower H/E) can show higher durability [6,24], although in other studies lower plasticity (i.e. higher H/E) and high H^3/E^2 have also been shown to be beneficial [25-27]. In the design of multilayer coatings for erosion protection Klemberg-Sapieha and co-workers have shown that increasing H^3/E^2 can be highly desirable [26-27]. A coating with high H^3/E^2

and lower elastic modulus than the substrate can spread the load over a larger volume. This can delay the onset of plastic deformation in the substrate and subsequent cracking and chipping of the coating due to the development of tensile stresses on the coating side close to the substrate-coating interface that result in cracks.

In this study the durability of TiFeN coatings on silicon to highly loaded sliding contact has been assessed using the nano-scratch test. The scratch test was initially thought of as primarily an adhesion test, with higher critical loads directly corresponding to more adherent films, but there is now a substantive body of evidence showing that it is the mechanical properties of the film and substrate that exert a significant influence on the deformation behaviour rather than the adhesion strength alone [28-38]. The critical load is dependent on many factors in addition to the interfacial strength. As noted in ASTM C1624 [38] the test method does not measure the fundamental "adhesion strength" of the bond between the coating and the substrate. Instead it "provides a quantitative engineering measurement of the practical (extrinsic) adhesion strength and damage resistance of the coating-substrate system as a function of applied normal force" [38]. One problem with the conventional (macro-scale) scratch test is that the probe radius (200 μm) is very large in comparison to the thickness of the coatings. The maximum von Mises stresses are typically far into the substrate at the critical load and substrate yield occurs before the coatings fail [39]. In a recent study, Wang and co-workers reported that the critical load for coating failure on a range of DLC and TiN coatings on titanium alloys did not depend on coating composition, but correlated directly with the hardness of the substrate [40]. The significance of substrate yield was emphasized by cross-sectional profiles of the scratch depth at failure which were much larger than the coating thickness.

The sensitivity of the scratch test to coating and interfacial properties can be increased by decreasing the probe radius and performing nano-scratch tests. We have previously reported that a-C [41], TiFeN [7] and nc-TiN/a-SiN_x [32] films deposited on silicon with high hardness can perform poorly in nano-scratch tests showing significant delamination extending far from the scratch track. However, in these previous studies it was not possible to fully determine the relationship between mechanical properties and scratch behaviour due to the limited number of samples tested. In this study a larger set of 18 TiFeN coatings were deposited on silicon by PVD with and without ion beam assistance (IBAD), with additional TiN and FeN films deposited for comparison. Although deposition rates are slower than in commercial PVD and CVD coating processes, the dual ion beam approach provides the flexibility and control of nitrogen content in the deposited films to obtain a wide range of mechanical properties. With this larger sample set it has proved possible, supported by high resolution SEM imaging, to investigate the relationship between mechanical properties and the scratch test critical load and deformation over a wide range of coating hardness and H^3/E^2. The variation in friction with increasing load has been investigated to understand the real contact area in sliding with the frictional response at failure providing the location of failure relative to the sliding probe. Analytical modelling of the main stresses was able to suggest how differences in coating mechanical properties affect the initial interface weakening (i.e. by initial substrate or coating yielding or both) and determine the deformation failure mechanism.

2. Experimental

2.1 Film deposition

A sample set of 18 (Ti,Fe)N_x films were deposited on pre-cleaned mirror polished Si (100) wafer substrates using a dual ion beam sputtering system described in detail previously [42].

Sputtering of the target was by a 1.25 keV Ar^+ ion beam with a 280-600 eV N_2^+ ion beam also used for ion-assistance of the deposited film in some cases. The sputter target comprised Ti and Fe with the area occupied by the Fe determining the relative Ti-Fe ratio in the coating. A thin Ti layer was initially deposited onto the Si surface to improve adhesion and the hard coating then deposited onto this bonding layer. Nitrogen ions from the second source bombarded the growing coating during ion-assisted nitride sputtering which occurred in a nitrogen partial pressure of 1-2 x 10^{-2} Pa. The substrate temperature was in the region 85-100 ^{0}C. Where films failed by delamination in the nano-scratch test it was possible to determine the film thickness and compare this with the thickness determined from SEM analysis of film cross-sections. Including the thin titanium interlayer the films were typically around 1.3 μm thick, with all being in the range 1.0-1.7 μm. For comparison FeN and TiN films were also deposited on silicon under similar conditions (the same thin Ti interlayer and similar overall film thickness).

2.2 Film characterisation

Nanoindentation and nano-scratch testing was performed using the Micro Materials NanoTest system. Multi-cycle load-controlled "load-partial-unload" experiments were performed up to 20 mN maximum load to assess the variation in mechanical properties with penetration depth. The unloading curves were analysed using standard methods with the area function for the Berkovich diamond indenter determined by indentations into fused silica. Film-only hardness was determined from the plateau (load-invariant) region and film-only elastic modulus by extrapolation to zero depth (following the extrapolation procedure outlined in ISO 14577-4 [43]). The reduced indentation modulus (E_r) can be converted to the Elastic modulus of the material according to Equation 2.

$$\frac{1}{E_r} = \frac{1-\nu_s^2}{E_s} + \frac{1-\nu_i^2}{E_i} \qquad [2]$$

Where E_s and E_i are the elastic moduli of the sample and indenter and ν_s and ν_i are the Poisson's ratios of the sample indenter respectively. In this paper E measurements are reported, after conversion of E_r to E using a Poisson ratio of 0.22. The H/E values of the TiFeN films are typically ~20% higher than their corresponding H/E_r values.

For the nano-scratch tests a well-used Berkovich indenter (end radius ~1000 nm) was used scratching edge-forward. An indenter was chosen with an end radius sufficiently rounded to avoid the possibility of indenter wear during the highly loaded scratches on the hard films. No evidence for indenter wear was found, as confirmed by subsequent re-testing showing the critical loads were unchanged. The NanoTest has high lateral stiffness minimising any influence of surface roughness so that scratch tracks remain smooth until film failure. The nano-scratch test involved three scans at 10 μm/s over a 600 μm track. In the initial (pre) and final (post) scans the applied load was 0.1 mN. In the second (progressive load scratch) scan the load was 0.1 mN for the first 0-100 μm and then linearly ramped at 10 mN/s to 500 mN. 5 repeat 3-scan scratch tests were done on each sample, with adjacent tracks separated by 50 μm. The first pre-scan at the 0.1 mN contact load was used to measure the film roughness. All the films had a low R_a roughness of 2-4 nm when measured over 100 μm. A Zeiss Supra40VP Field Emission Gun SEM system was used for the high-resolution microscopy. Film thickness was determined using SEM analysis of fracture sections. All films exhibited a dense microstructure. The TiN and FeN films had a pronounced columnar morphology which was much less marked/absent in the TiFeN films. The von Mises, tensile and shear stresses acting on the coating and substrate sides of the interface were evaluated using the SAC (simple adhesion calculator) in the SIO Toolbox (SIO, Rugen, Germany) which uses Film

Doctor (SIO, Rugen, Germany) analytical methodology to determine the main stresses acting on the interface for a single-layer coating system.

3. Results

3.1 Nanoindentation

The TiFeN films exhibited a wide range of mechanical properties, with the hardness varying from 13.1-29.3 GPa and the elastic modulus from 233-375 GPa as summarised in Table 1. Increasing ion bombardment typically resulted in a reduction in film hardness. Harder films were also higher in stiffness so that the corresponding variation in H/E was relatively small at 0.056-0.081. However, the parameter H^3/E^2 varied more strongly from 0.041-0.188 GPa. The comparative TiN films were harder and stiffer than the TiFeN films. The FeN films had hardness and stiffness that were comparable with some of the Fe(Ti)N_x films. All films were higher in stiffness than the silicon substrate.

3.2 Nano-scratch testing

A ductile response was observed for Fe(Ti)N and FeN films produced with low hardness and very low H^3/E^2, as illustrated for FeN in Figure 1(a). Failure was cohesive with ductile chipping at the edges of the scratch track although there were no dramatic coating failures. For some of the films with hardness ~15 GPa the ductile deformation was accompanied by delamination from the side of the scratch track. Incorporating more Ti in the film increased the hardness (~20 GPa) and in the scratch test delamination events were observed that were accompanied by fluctuations in the friction force. For TiFeN films with higher hardness periodic fine cracks were observed in the scratch track. At high load a more localised brittle machining mode is accompanied by a delamination failure in the wake of the contact zone as

illustrated in Figure 1(b). Films deposited with very high H^3/E^2 showed either brittle machining failure (Figure 1(c)) or adhesion failure at low load (Figure 1(d)).

Examination of the residual scratch depth data showed that plastic deformation occurred below 2 mN on all the films. The L_{c1} (cracking) critical load was difficult to determine from the on-load scratch depth or friction data so microscopy and analysis of residual depth data were used. For many of the films L_{c1} was ~ 50 mN although higher values were found for some of the films, particularly those with higher H^3/E^2. Scratch recovery was ~75 % for films with higher H/E and H^3/E^2. The more ductile Fe(Ti)N and FeN films showed lower scratch recovery (~50-60 %) and a clear L_{c2} failure was not generally observed. The L_{c2} critical load for coating failure in the nano-scratch test was determined from the depth and friction data. Figures 2(a,b) show how this varied with the H/E and H^3/E^2 ratio of the coatings for all the (non-ductile) coatings that exhibit clear L_{c2} failure. The highest L_{c2} critical loads were obtained for TiFeN films with H ~ 25 GPa, H/E ~ 0.075 and H^3/E^2 ~ 0.13 GPa. The three hardest coatings tested exhibited a dramatic unloading failure in the vicinity of L_{c1} (50-100 mN).

The friction coefficient between the diamond probe and the more ductile films [(Fe,Ti)N_x and FeN] was typically 0.25-0.30 and slightly less (0.2-0.25) on all the harder films. The variation in friction coefficient vs. load is illustrated in Figure 3(a) for TiFeN films with H^3/E^2 = 0.09-0.188 GPa and TiN films with H^3/E^2 = 0.133 GPa and 0.149 GPa. The expanded view of the data in the first 70 mN is shown in Figure 3(b). For these TiFeN films the friction coefficient increased with load over the first 0-70 mN thereafter remaining virtually constant. The friction force was rather insensitive to the film failure when film failure occurred by delamination or brittle machining initiating behind the probe. There was no apparent

correlation between the friction force at L_{c2} film failure (0.22-0.25) and the film mechanical properties. The frictional forces exhibited a high level of reproducibility in the repeat tests as illustrated in Figure 4 for (a) TiFeN with film H^3/E^2 = 0.13 GPa (b) TiFeN with film H^3/E^2 = 0.060 GPa (for clarity only 3 of the 5 repeats are shown). The friction force changes little at film failure in both cases (critical load = 250 mN in 4(a) and 160 mN in 4(b)) with the onset of oscillations around 300 mN being due to fracturing of the silicon substrate.

4. Discussion

The (Ti,Fe)N_x films were produced with a wide range of mechanical properties to a maximum hardness of 29.3 GPa. Increasing ion assistance during deposition decreases hardness and stiffness of the films in agreement with our previous report that ion assistance produces softer TiFeN films when accompanied by compositional changes [7,44]. Adding iron into TiN films can either lead to inclusions of Fe or FeN_x clusters [46]. In both cases the inclusions are much softer than TiN matrix and provide plastic zones within the stiff matrix. With increasing ion assistance more Fe (and hence FeN) and more N were present in the films. Compositional analysis studying the effects of ion assistance on (Ti,Fe)N_x films [7,44] showed that the Fe/Ti ratio in the films was 0.4 without ion assistance rising to 0.63-0.7 with ion assistance. The Ti/N ratio varied from 1.3 without ion assistance to 1.9. Fe and FeN in (Ti,Fe)N_x films are expected to contribute to the decrease in hardness. The general trend that the parameter H^3/E^2 varied with film composition more widely than H or H/E is consistent with previous reports on hard nitride coatings by Musil [10,21,45].

The results summarised in Figure 2 provide further evidence that the nano-scratch test does not measure the fundamental adhesion strength of the bond between the coating and the substrate. Although all the films would be expected to have similar interfacial bonding strength due to the same thin Ti bonding layer and Si substrate, it is clear that the mechanical

properties of the films strongly influence the critical load, location and type of failure in the test. Similar trends in critical load were found vs. H, H/E and H^3/E^2. The parameter H^3/E^2 varied with film composition more widely than H or H/E so its variation was used to investigate the influence of mechanical properties on the critical load in the nano-scratch test. Figure 1(a-d) and Figure 2(c) show the coating behaviour can be broadly divided into (i) films with low H^3/E^2 that display ductile behaviour without a clear L_{c2} before the 500 mN maximum load in the test is reached (ii) films with low to intermediate H^3/E^2 (iii) optimum behaviour at intermediate-to-high H^3/E^2 and (iv) a marked reduction in critical load for films with very high H^3/E^2. Plastic flow can be considered as a major source of stress relaxation in the coating system. The presence of softer plastic zones blunts the cracks and slows down their propagation by ductile phase deformation and (potentially) crack bridging [17]. Increasing Fe and FeN in these TiFeN films can effectively toughen them but at expense of their hardness. Higher critical loads together with more ductile deformation have also been reported in the nano- [41] micro- [47] and macro-scale [48-49] scratch tests on soft (~10 GPa) metal-doped carbon coatings. Fratzl and co-workers have also shown toughness enhancement in materials with spatial variation in elastic modulus [50-51]. This is due to a strong decrease in crack driving force which leads to crack propagation being retarded or crack arrest when the crack tip reaches regions of low modulus. Both Fe and FeN have lower stiffness than TiN films so spatial modulus variation may also contribute to the toughening effect in the more ductile and Fe and FeN rich TiFeN when a degree of phase separation is likely.

As the hardness increases to ~20 GPa, with low to intermediate H^3/E^2, the films display predominantly ductile scratch tracks prior to failure (Figure 1(b)) but significant interfacial stresses can exist and film delamination occurs at moderate load. Increasing H and H^3/E^2

results in periodic small cracks at the centre and edges of the scratch track. These cracks do not extend to the edges of the scratch track, so may be non-propagating, enabling high critical load. Films deposited with very high H^3/E^2 have higher hardness (29-31 GPa) and load-carrying ability but limited plasticity. When films were deposited with very high H^3/E^2 and the interfacial adhesion is strong the strain accumulation as the load increases in the scratch test results in regular cracks within the scratch track. The fine scale cracking and very slight undulations in the track may act as dissipative mechanisms although they are not as effective as the more pronounced undulations in the track indicative of some stick-slip that were observed previously on TiFeMoN films that were highly resistant to delamination in the nano-scratch test [7]. As the load increases the very high H^3/E^2 films with limited plasticity or other stress relieving mechanisms undergo dramatic brittle machining of the Si substrate. However, when adhesion is weak failure can occur at low load. The decrease in critical load when films were deposited with H^3/E^2 >0.13 GPa has also been observed on nc-TiN/a-SiN_x films deposited on silicon in nano-scratch tests performed with a spheroconical indenter with end radius R = 3 μm [32]. In that study pronounced failure occurring behind the probe was only observed for films with higher H/E and H^3/E^2, being most dramatic for a film with hardness of 29 GPa and H^3/E^2 = 0.183 GPa. The role of tensile stresses in these failures is discussed below with support from the friction measurements.

The load dependence of the friction coefficient provides (i) evidence for the real contact area during the sliding contact (specifically whether the load is being supported predominantly on the front half of the sliding probe or whether contact more elastic and the load more evenly distributed) (ii) an indication of the location of failure relative to the sliding probe. Prior to coating failure the dependence of the friction coefficient on the applied load is a consequence of: (i) the increasing ploughing contribution as the scratch depth increases and (ii) the

geometric change from the rounded spherical tip to the Berkovich geometry, and further away from elastic contact, as the scratch depth increased with applied load. The friction force in a scratch test is a product of interfacial and ploughing components [52-54] (Eqn. 3):-

$$\mu_{\text{total}} = \mu_{\text{interfacial}} + \mu_{\text{ploughing}} \qquad \text{[Eqn. 3]}$$

In contrast to scratch tests with larger end radii probes where the interfacial friction can play a more dominant role, when small spherical probes or Berkovich indenters are used in the nano-scratch the ploughing contribution can be more significant. Due to the high lateral rigidity of the test instrumentation used in this study the friction forces were extremely reproducible (Figure 4a,b) so it is possible to reliably deconvolute these contributions. Provided there is sufficient frictional resolution the interfacial friction component can be estimated by the value at low load where the on-load scratch depth is minimal and the contribution from ploughing is negligible. The low load data for the TiN films in Figure 4 (b) suggest a value around 0.05-0.06 in good agreement with previous determinations in the literature, which typically range from 0.04-0.08 for 0.5-5 μm TiN coatings sliding against diamond probes with end radii of 5-200 μm, or against cemented carbide with an end radius of 350 μm [30-31, 54-57]. For the well-worn Berkovich used for these tests the variation in friction in Figure 4(b) can split into different regimes (i) 0-10 mN the friction is controlled by the spherical end cap (ii) 10-70 mN – transition to the Berkovich geometry (iii) Berkovich geometry (70 mN to film failure). Based on the relative projected areas in the normal and sliding directions it is possible to estimate the ploughing contribution to the friction coefficient for an ideal Berkovich scratching edge-on as ~0.22 when only the front face of the sliding indenter carries the load [58]. However, elastic recovery can play an important role in the friction of sliding indenters [53]. The value of 0.22 should be considered as an upper bound since the residual scratch depth data show that there is significant elastic recovery (~75

%) and therefore the normal load is not being solely supported on the front half of the probe. The experimental friction measurements are in good agreement with these predictions. For all the TiN and TiFeN films shown in Figure 4(b) the friction at failure, for example, is ~0.23 composed of contributions from $\mu_{interfacial}$ ~0.05 and $\mu_{ploughing}$ ~0.18. On the more ductile films the friction coefficient is larger, due to lower scratch recovery and the load being supported more on the front half of the sliding probe. Although the magnitude of the friction force at failure does not clearly discriminate between the harder films the presence or absence of oscillations in the frictional signal at failure provides strong additional evidence on the location of the first failure relative to the sliding contact region. Marked oscillations in the friction were observed when failure occurs either in front or, or at the front/side of the moving scratch probe, as was noted in our previous report on behaviour of TiFeN films in the nano-scratch test [7] and also observed on lower hardness TiN coatings on M42 steel that also fail in front of the probe [56]. In contrast, in many of the TiFeN films studied here failure was barely noticeable in the friction force (e.g. see Figure 3(a), 4(a,b)) despite leading to large-area delamination in many cases. This confirms that the failure in these cases initially occurs behind the probe, as was suggested in reference 7. Finite element modelling of the first principal stress in scratch testing of TiN on high speed steel has shown that there is a tensile stress maximum at the surface at a distance of around half-contact width behind the sliding contact [31]. The position behind the probe (rather than at the trailing edge of the contact) is consistent with the cracking not being observed in the friction force. The magnitude of the tensile stress at the coating side of the interface has been estimated using the SAC (simple adhesion calculator) in the SIO Toolbox. This uses analytical methodology to determine the main stresses acting on the interface (von Mises, tensile and shear stresses) for a single-layer coating system. The input parameters are the mechanical properties of the coating and substrate i.e. *H*, *E*, *H*/*Y* (for simplicity assumed to be 1.5 for the coatings and 1

for the silicon substrate), their Poisson ratios, together with the applied load, friction coefficient and probe radius in the nano-scratch test. For the analysis the coating thickness was 1.3 μm and the friction coefficient was 0.2. For the ~1 μm end radius probe used in this study it was possible to accurately determine the stresses at the low scratch depths at which the deformation was dominated by the end radius, which the friction data suggest is up to ~60 mN. The SAC analysis shows that at 50 mN (~L_{c1}) there is plastic flow constrained within the coating. Substrate yield does not occur over the load range which the analysis is applicable (to ~60 mN for the 1 μm probe). The results show that significant tensile stresses are present on the coating side of the interface at low load and the peak von Mises stress on the substrate side rapidly approaches the substrate yield strength as the load increases. Figure 5 shows the evolution of the tensile stress with (a) load for a sub-set of the coatings and (b) hardness for all of these coatings at 50 mN. Three of the coatings tested exhibit a dramatic unloading failure at low load (50-100 mN). These are the TiN coatings and the hardest TiFeN coating which the stress analysis show have the highest tensile stresses which increase more rapidly with load. The results are consistent with failure on these coatings being due to a combination of high tensile stress and substrate yield. On the softer coatings there is a different failure mechanism. Yield begins within the coating at lower tensile stress, and the interface is weakened from the coating side which does not result in the same dramatic unloading failures as when the interface is weakened first by substrate yield. Analysis of previously reported data on ~0.42-1.1 μm nc-TiN/a-SiN_x films on Si when scratched by a R = 3 μm spheroconical probe has shown similar trends in deformation mechanism with coating mechanical properties [32].

The experimental and modelling results show that mechanical properties of the coating, its thickness and the substrate properties all influence the deformation in the nano-scratch test.

When hard coatings are deposited on silicon increasing thin film hardness, H/E and H^3/E^2 beyond a critical point results in a decrease in scratch test critical load. The differences in coating mechanical properties affect how the interface is weakened (i.e. by initial substrate or coating yielding or both) and determine the deformation failure mechanism.

A complex stress state exists during highly loaded sliding in the nano-scratch test. A simpler contact geometry exists during indentation where high fracture toughness has been correlated to high H/E or H^3/E^2 [59-60]. On the basis of these and other studies it has been suggested that coatings should be designed to be as hard as possible with very high H/E and H^3/E^2 to be crack resistant, although this runs counter to the usual antagonism between hardness and toughness. It may be primarily a consequence of the higher load-support as the critical load for plastic flow is correlated with H^3/E^2 [9]. At a given load the substrate deformation is lower so the bending stresses in the coating are reduced and it may be this, rather than intrinsic structural toughening, that results in higher apparent toughness in the indentation test. Musil and co-workers have reported that nanocomposite coatings should have a combination of low elastic modulus and $H/E^* > 0.1$ to be crack resistant in indentation ($E^* = E/(1-\nu^2)$) [21,61]. For the Al-Cu-O and nc-(γ-Al(Cu)O_2/a-Al_2O_3 coatings they studied, moderate hardness was combined with low stiffness. The lower modulus of the coatings, which reduces the modulus mismatch with the substrate, may be an equally important factor in their crack resistance.

Several authors have investigated the correlation between the critical load in a scratch test and toughness [15-20,32,63]. Zabinski and Voevodin proposed that the lower critical load in a scratch test could provide a measure of the fracture toughness [62]. This concept was later extended by Zhang and co-workers [17-20] who equated L_{c1} with the resistance to the

initiation of cracks and (L_{c2}-L_{c1}) as a measure of crack propagation (L_{c2} = load for total coating failure). They proposed a parameter (later termed "scratch toughness" [17,19,20]) representing a combined resistance to crack initiation and propagation:-

$$\text{Scratch toughness} = L_{c1}(L_{c2}\text{-}L_{c1}) \qquad [4]$$

Values of the scratch toughness are inevitably a function of the geometry of the scratch probe (increasing with probe radius) making them difficult to compare between studies. Nevertheless, they provide a useful qualitative assessment of coating behaviour and have been used in several studies aimed at developing "hard yet tough" coatings. The relationship between scratch toughness and H^3/E^2 of the (Ti,Fe)N_x films is shown in Figure 6. The scratch toughness definition accounted for the possibility of unloading failure, as was done previously in nano-scratch testing of nc-TiN/a-Si_3N_4 films where unloading failures (L_u) also can occur [32]. The critical load for coating failure (L_{tf}) was taken as the lower value of either L_{c2} or the unloading failure (L_u) so that scratch toughness was defined as:-

$$\text{Scratch toughness} = L_{c1}(L_{tf}\text{-}L_{c1}) \qquad [7]$$

For the ductile films that do not display an L_{c2} before the maximum load of the scratch test (500 mN) a lower bound for the scratch toughness is 22500 mN^2. This high scratch toughness is consistent with the more localised deformation and lower chipping in the scratch test. For the films exhibiting at clear L_{c2} failure a maximum in scratch toughness (~20000 mN^2) was found for films with H^3/E^2 ~ 0.13 GPa and hardness around 25 GPa. For metal-doped carbon coatings on steel substrates improved scratch toughness has usually been associated with a significant decrease in coating hardness compared to undoped coatings. The highest scratch

toughness was for carbon films with *H* ~10-12 GPa [47-49]. Similarly, Zhang and co-workers reported improvements in scratch toughness that were at the cost of hardness in metal-doped nc-Me_nN/a-SiN_x coating systems [17-20, 63]. Nickel addition to hard CrAlN/a-SiN_x nanocomposite coatings typically decreases hardness, and at 12 at.% Ni a reduction to *H* ~18 GPa was able to provide a x5 improvement in scratch toughness compared to undoped CrAlN/a-SiN_x nanocomposites with *H* ~27 GPa [63]. A maximum in the scratch toughness of nc-TiN/a-Si_3N_4 films produced by magnetron sputtering [18] or ion beam assisted deposition [32] has been found at *H* ~20 GPa.

The enhanced toughening in the nano-scratch tests of TiFeN at intermediate hardness appears to be due to a combination of factors:- (i) dense nanocomposite microstructure removing the weak columnar boundaries present in TiN (ii) avoidance of the high tensile stresses that develop in the nano-scratch testing of the hardest films (iii) sufficient hardness (iv) localised energy dissipative mechanisms. For the more ductile films the presence of soft and low stiffness inclusions has a further beneficial effect.

However, TiFeMoN coatings previously tested under similar conditions [10] provided more effective stress relief by a combination of localised energy dissipative processes - intergranular fracture, micro-cracking and stick slip – than the TiFeN films described in this study. It was suggested in [7] that coatings that show high toughness should combine (1) a high load threshold for the initiation of cracking (2) mechanisms to minimise and retard crack propagation – i.e. it is necessary to display a certain degree of damage tolerance. Designing thin films with in-built dissipative structures and mechanisms to combat stress (i.e. self-adaptive behaviour [64-66]) is a more successful route to optimise their toughness than aiming to minimise plasticity by increasing their hardness. Operation in extreme

environments, such as high temperature, invariably leads to changes that can result in the segregation of some components with or without considerable losses of volatile components and/or oxidation in the near-surface layers. The latest developments can be seen in refs. [66,67] for example. The point is that a protective coating can separate into nanostructured phases with different properties. Potentially this can significantly modify material crack resistance both ways – either increasing crack resistance or making the material more prone to cracking. Understanding and managing this process will be beneficial to emerging engineering applications. Although there has been much research into super-hard coatings [68-70] in general their performance in practical wear situations has been unconvincing as yet. The modelling in this study has shown that in the scratch test even a coating hardness of ~30 GPa is sufficient to generate high tensile stresses on the coating side of the coating-interface which the experimental results show can lead to dramatic interfacial failures at relatively low load.

In mechanical contacts, including laboratory mechanical tests such as nanoindentation, nano-scratch, or nano-impact, there is a balance between load-support (~hardness) and crack resistance (toughness) that controls the observed deformation behaviour. Coating design based on optimising a number of factors rather than solely aiming to maximise hardness and resistance to plastic deformation can be more effective. Details of the mechanical contact conditions in each test differ altering the relative importance of hardness and toughness. In an indentation test high hardness and H^3/E^2 can be more important than in highly loaded sliding in the nano-scratch test.

5. Conclusions

A complex stress state exists during highly loaded sliding in the nano-scratch test. Experimental and modelling results on (Ti,Fe)N_x films show that mechanical properties of the coating, its thickness and the substrate properties all influence the deformation. They affect the critical loads required, the type of failures observed and their location relative to the sliding probe. Differences in coating mechanical properties affect how the interface is weakened (i.e. by initial substrate or coating yielding or both) and determine the deformation failure mechanism.

Introduction of soft, low elastic modulus inclusions in thin TiFeN films by increasing Fe and N content led to better crack resistance and effective toughness in sliding contact but at a large cost to the coating hardness. In practical applications coatings often need to be sufficiently hard as well as tough. Increasing the hardness by decreasing or eliminating ion assistance during deposition decreased the ductility but led to a maximum in critical load at H^3/E^2 ~0.13 GPa. Harder films with higher H^3/E^2 behaved poorly with extensive delamination outside the scratch track at low load. Analytical stress modelling suggested this was a consequence of very high tensile stresses on the coating side at the interface with the substrate.

6. Acknowledgements

Professor John Colligon (University of Huddersfield) is acknowledged for his valuable support and suggestions.

7. References

1. A. Leyland and A. Matthews, Design criteria for wear-resistant nanostructured glassy-metal coatings, Surf. Coat. Technol. 177-178 (2004) 317-324.
2. A. Leyland and A. Matthews, On the significance of the H/E ratio in wear control: a nanocomposite coating approach to optimised tribological behaviour, Wear 246 (2000) 1-11.
3. Y.-T. Cheng and C.-M. Cheng, Relationships between hardness, elastic modulus, and the work of indentation, Appl. Phys. Lett. 73 (1998) 614-616.
4. Y.-T. Cheng and C.-M. Cheng, Scaling, dimensional analysis, and indentation measurements, Mater. Sci. Eng. R 44 (2004) 91-149.
5. G.S. Fox-Rabinovich, S.C. Veldhuis, V.N. Scvorstov, L.S. Shuster, G.K. Dosbaeva, Elastic and plastic work of indentation as a characteristic of wear behavior for cutting tools with nitride PVD coatings, Thin Solid Films, 469-470 (2004) 505.
6. B.D. Beake, G.S. Fox-Rabinovich, S.C. Veldhuis and S.R. Goodes, Coating optimisation for high-speed machining with advanced nanomechanical test methods, Surf. Coat. Technol. 203 (2009) 1919-1925.
7. B.D. Beake, V.M. Vishnyakov, and A.J. Harris, Relationship between mechanical properties of thin nitride-based films and their behaviour in nano-scratch tests, Tribol. Int. 44 (2011) 468.
8. A.J. Harris, B.D. Beake, D.E.J. Armstrong and M.I. Davies, Development of high temperature nanoindentation methodology and its application in the nanoindentation of polycrystalline tungsten in vacuum to 950 ºC, Exp. Mech. (2016) DOI 10.1007/s11340-016-0209-3.
9. K.L. Johnson, Contact Mechanics, Cambridge University Press, London, UK, 1985, ISBN: 0-521-34796-3, p.464.

10. J. Musil. Physical and Mechanical Properties of Hard Nanocomposite Films Prepared by Reactive Magnetron Sputtering. in Nanostructured coatings, eds. A. Cavaleiro and J.Th.M. De Hosson, Springer, New York 2006, pp407-463.
11. S. Zhang, H.L. Wang, S.-E. Ong, D. Sun and X.-L. Bui, Hard yet tough nanocomposite coatings – present status and future trends, Plasma Process. Polym. 4 (2007) 219-228.
12. J. Musil and M. Jirout, Toughness of hard nanostructured ceramic thin films, Surf. Coat. Technol. 201 (2007) 5148-5152.
13. D.G. Sangiovanni, V. Chirita, and L. Hultman, Toughness enhancement in TiAlN-based quarternary alloys, Thin Solid Films 520 (2012) 4080-4088.
14. D.G. Sangiovanni, L. Hultman, and V. Chirita, Supertoughening in B1 transition metal nitride alloys by increased valence electron concentration, Acta Mater. 59 (2011) 2121-2134.
15. S. Zhang, X.L. Bui, Y. Fu and H. Du, Development of carbon-based coating on extremely high toughness with good hardness, Int. J. Nanosci. 3 (2004) 571-578.
16. S. Zhang, X.L. Bui, Y. Fu, D.L. Butler and H. Du, Bias-graded deposition of diamond-like carbon for tribological applications, Diam. Relat. Mater. 13 (2004) 867-871.
17. Y.X. Wang and S. Zhang, Toward hard yet tough ceramic coatings, Surf. Coat. Technol. 258 (2014) 1-16.
18. S. Zhang, D. Sun, Y. Fu and H. Du, Effect of sputtering target power on microstructure and mechanical properties of nanocomposite nc-TiN/a-SiNx thin films, Thin Solid Films, 447–8 (2004) 462-467.
19. Y.X. Wang and S. Zhang, Present status of hard-yet-tough ceramic coatings, Chapter 1, pp1-45 in Thin Films and Coatings: Toughening and Toughness Characterisation, ed. S Zhang, CRC Press, July 2015, p15.

20. X. Zhang, B.D. Beake and S. Zhang, Toughness Evaluation of Thin Hard Coatings and Films, Chapter 2, pp48-121 in Thin Films and Coatings: Toughening and Toughness Characterisation, ed. S Zhang, CRC Press, July 2015, p53.
21. J. Musil, Advanced hard coatings with enhanced toughness and resistance to cracking, Chapter 7, pp378-463 in Thin Films and Coatings: Toughening and Toughness Characterisation, ed. S Zhang, CRC Press, July 2015, p383.
22. Z. Li, P. Munroe, Z.-T. Jiang, X. Zhao, J. Xu, Z.-F. Zhou et al, Designing superhard, self-toughening CrAlN coatings through grain boundary engineering, Acta Mater. 60 (2012) 5735–5744.
23. J. Xu, Z.-Y. Li, Z.-H. Xie and P. Munroe, Uniting superhardness and damage-tolerance in a nanosandwich-structured Ti–B–N coating, Scr. Mater. 74 (2014) 88–91.
24. G.S. Fox-Rabinovich, B.D. Beake, S.C. Veldhuis, J.L. Endrino, R. Parkinson, L.S. Shuster, M.S. Migranov, Impact of mechanical properties measured at room and elevated temperatures on wear resistance of cutting tools with TiAlN and AlCrN coatings, Surf Coat Technol 200 (2006) 5738-5742.
25. B.D. Beake, G.S. Fox-Rabinovich, Y. Losset, K. Yamamoto et al, Why can TiAlCrSiYN-based adaptive coatings deliver exceptional performance under extreme frictional conditions? Faraday Discussions 156 (2012) 267-278.
26. S. Hassani, M. Bielawski, W. Beres, L. Martinu, M. Balazinski and J. E. Klemberg-Sapieha, Predictive tools for the design of erosion resistant coatings, Surf. Coat. Technol. 203 (2008) 204–210.
27. E. Bousser, M. Benkahoul, L. Martinu and J.E. Klemberg-Sapieha, Effect of Microstructure on the Erosion Resistance of Cr-Si-N Coatings, Surf. Coat. Technol. 203 (2008) 776-780.

28. M. Larsson, M. Olsson, P. Hedenqvist and S.Hogmark, Mechanisms of coating failure as demonstrated by scratch and indentation testing of TiN coated HSS – On the influence of coating thickness, substrate hardness and surface topography, Surf. Eng. 16 (2000) 436-444.
29. H. Ichimura and Y. Ishii, Effects of indenter radius on the critical load in scratch testing. Surf. Coat. Technol. 165 (2003) 1-7.
30. K. Holmberg, H. Ronkainen, A. Laukkanen and K. Wallin, Friction and wear of coated surfaces – scales, modelling and tribomechanisms, Surf. Coat. Technol. 202 (2007) 1034-1049.
31. K. Holmberg, H. Ronkainen, A. Laukkanen and K. Wallin, A. Erdemir and O. Eryilmaz, Tribological analysis of TiN and DLC coated contacts by 3D FEM modelling and stress simulation, Wear 264 (2008) 877-884.
32. B.D. Beake, V.M. Vishnyakov, R. Valizadeh and J.S. Colligon, Influence of mechanical properties on the nanoscratch behaviour of hard nanocomposite TiN/Si_3N_4 coatings on Si, J. Phys. D: Appl. Phys. 39 (2006) 1392-1397.
33. P.A. Steinmann, Y. Tardy and H.E Hintermann, Adhesion testing by the scratch test method: influence of intrinsic and extrinsic parameters on the critical load, Thin Solid Films 154 (1987) 333-49.
34. H. Ollendorf and D. Schneider, A comparative study of adhesion test methods for hard coatings, Surf. Coat. Technol. 113 (1999) 86-102.
35. S.J. Bull and D.S. Rickerby, New developments in the modelling of the hardness and scratch adhesion of thin films, Surf. Coat. Technol. 142 (1990) 149-164.
36. P.J. Burnett and D.S. Rickerby, The relationship between hardness and scratch adhesion, Thin Solid Films 154 (1987) 403-416.

37. S.J. Bull, Failure modes in scratch adhesion testing, Surf. Coat. Technol. 50 (1991) 25-32.
38. ASTM C1624-05(2015), Standard Test Method for Adhesion Strength and Mechanical Failure Modes of Ceramic Coatings by Quantitative Single Point Scratch Testing.
39. N. Schwarzer, Q.-H. Duong, N. Bierwisch, G. Favaro, M. Fuchs, P. Kempe, B. Widrig and J. Ramm, Optimisation of the scratch for specific coating designs, Surf. Coat. Technol. 206 (2011) 1327-1335.
40. C.T. Wang, A. Escudeiro, T. Polcar, A. Cavaleiro and R.J.K. Wood, Indentation and scratch testing of DLC-Zr coatings on ultrafine-grained titanium processed by high-pressure torsion, Wear 2013 (306) 304-310.
41. B. Shi, J.L. Sullivan and B.D. Beake, An investigation into which factors control the nanotribological behaviour of thin sputtered carbon films, J Phys D:Appl Phys 41 (2008) 045303.
42. J.S. Colligon, V.M. Vishnyakov, R. Valizadeh, S.E. Donnelly and S. Kumashiro, Study of nanocrystalline TiN/Si_3N_4 thin films deposited using a dual ion beam method. Thin Solid Films 485 (2005) 148-154.
43. ISO 14577: Metallic Materials – Instrumented Indentation Test for Hardness and Materials Parameters, Part 4 - Test Method for metallic and non-metallic coatings.
44. B.D. Beake, V.M. Vishnyakov and J.S. Colligon, Nano-impact testing of TiFeN and TiFeMoN films for dynamic toughness evaluation, J Phys D: Appl Phys 44 (2011) 085301.
45. J. Musil, H. Polakova, J. Suna and J. Vlcek, Effect of ion bombardment on properties of hard reactively sputtered Ti(Fe)N_x films. Surf. Coat. Technol. 177-178 (2004) 289-298.
46. B.M. Biwer and S.L. Bernasek, Investigation of the electronic structure of an iron-titanium nitride ammonia synthesis catalyst, Appl. Surf. Sci. 25 (1986) 41–52.

47. B.D. Beake, T.W. Liskiewicz, V.M. Vishnyakov and M.I. Davies, Development of DLC coating architectures for demanding functional surface applications through nano- and micro-mechanical testing, Surf. Coat. Technol. 284 (2015) 334-343.
48. K. Vercammen, H. Haefke, Y. Gerbig, A. Van Hulsel, E. Pfluger and J. Meneve, A comparative study of state-of-the-art diamond-like carbon films, Surf. Coat. Technol. 133-134 (2000) 466-472.
49. J. Meneve, D. Havermans, K. Vercammen, H. Haefke, Y. Gerbig and E. Pfluger, Mechanical properties and tribological behaviour of State-of-the-art diamond-like carbon films, Adv. Mater. 3 (2001) 163-166.
50. P. Fratzl, H.S. Gupta, F.D. Fischer and O. Kolednik, Hindered crack propagation in materials with periodically varying Young's modulus – lessons from biolological materials, Adv. Mater. 19 (2007) 2657-2661.
51. O. Kolednik, J. Predan, F.D. Fischer and P. Fratzl, Improvements of strength and fracture resistance by spatial material property variations, Acta Mater. 68 (2014) 279-284.
52. F.P. Bowden and D. Tabor, The friction and lubrication of solids, Oxford University Press, Oxford, UK, 1986, p. 374.
53. J.-D. Kamminga and G.C.A.M. Janssen, Experimental discrimination of ploughing friction, Tribol. Lett. 25 (2007) 149-152.
54. H. Ronkainen, A. Laukkanen, K. Holmberg, Friction in a coated surface deformed by a sphere, Wear, 263 (2008) 1315-1323.
55. K. Dryda K and M. Sayer, Critical loads and effective frictional force measurements in the industrial scratch testing of TiN on M2 tool steel, Thin Solid Films 355-356 (1999) 277-283.
56. B.D. Beake, B. Shi and J.L. Sullivan, Nanoscratch and nanowear testing of TiN coatings on M42 steel, Tribology 5 (2011) 141-147.

57. J.F. Smith, V.M. Vishnyakov, M.I. Davies and B.D. Beake, Nanoscale Friction Measurements Up to 750 °C, Tribol. Lett. 49 (2013) 455-463.
58. F. Zhang, B. Meng, Y. Geng, Y. Zhang and Z. Li, Friction behaviour in nanoscratching of reaction bonded silicon carbide ceramic with Berkovich and sphere indenters, Tribol. Int. 97 (2016) 21-30.
59. Y.T. Pei, D. Galvan and J.Th.M. De Hosson, Nanostructure and properties of TiC/a-C:H composite coatings, Acta Materialia 53 (2005) 4505-4521.
60. D. Galvan, Y.T. Pei and J.Th.M. De Hosson, Deformation and failure mechanism of nano-composite coatings under nanoindentation, Surf. Coat. Technol. 200 (2006) 6718-6726.
61. J. Musil, Hard nanocomposite coatings: thermal stability, oxidation resistance and toughness, Surf. Coat. Technol. 207 (2012) 50-65.
62. A.A. Voevodin and J.S. Zabinski, Load-adaptive crystalline-amorphous nanocomposites, J. Mater. Sci. 33 (1998) 319-327.
63. Y.X. Wang, S. Zhang, J.-W. Lee, W.S. Lew and B. Li, Toughening effect of Ni on nc-CrAlN/a-SiN_x hard nanocomposite, Appl. Surf. Sci. 265 (2013) 418-423.
64. A.A. Voevodin, J.J. Hu, J.G. Jones, T.A. Fitz and J.S. Zabinski, Growth and structureal characterisation of yttria-stabilised zirconia-gold nanocomposite films with improved toughness, Thin Solid Films 410 (2001) 187-195.
65. A.A. Voevodin and J.S. Zabinski, Nanocomposite and nanostructured tribological materials for space applications, Comp. Sci. Technol. 65 (2005) 741-748.
66. A.A. Voevodin, C. Muratore and S.M. Aouadi, Hard coatings with high temperature adaptive lubrication and contact thermal management: review, Surface and Coating Technol. 257 (2014) 247-265.

67. P. Zeman P. Zeman, Š. Zuzjaková, P. Mareš, R. Čerstvý, M. Zhang, J. Jiang, E.I. Meletis and J. Vlček, Superior high-temperature oxidation resistance of magnetron sputtered Hf-B-Si-C-N film, Ceramics International 42 (2016) 4853-4859.
68. S. Veprek and M.G.J. Veprek-Heijman, Concept for the Design of Superhard Nanocomposites with High Thermal Stability: Their Preparation, Properties, and Industrial Applications, in Nanostructured coatings, eds. A. Cavaleiro and J.Th.M. De Hosson, Springer, New York 2006, pp.347-406.
69. S. Veprek, The search for novel, superhard materials, J. Vac. Sci. Technol. A 17 (1999) 2401-2420.
70. S. Veprek, A. Niederhofer, K. Moto, T. Bolom, H-D. Männling, P. Nesladek et al, Composition, nanostructure and origin of the ultrahardness in nc-TiN/a-Si_3N_4 and nc-$TiSi_2$ nanocomposites with H_v = 80 GPa to ≥105 GPa, Surf. Coat. Technol. 133-134 (2000) 152-159.

Table 1 Composition and mechanical properties of the (Ti,Fe)N_x thin films

Film	Ion assist/V	*H* (GPa)[§]	*E* (GPa)[§]	*H*/*E*	H^3/E^2 (GPa)
TiN	-	31.0	474	0.065	0.133
TiN	-	30.0	426	0.070	0.149
(Ti,Fe)N_x	-	23.5	312	0.075	0.133
(Ti,Fe)N_x	-	29.3	366	0.080	0.188
(Ti,Fe)N_x	-	25.0	307	0.099	0.165
(Ti,Fe)N_x	-280 V	23.7	311	0.076	0.138
(Ti,Fe)N_x	-300 V	26.0	375	0.069	0.125
(Ti,Fe)N_x	-300 V	26.0	330	0.079	0.162
(Ti,Fe)N_x	-300 V	21.0	320	0.066	0.090
(Ti,Fe)N_x	-600V	14.0	211	0.075	0.061
(Ti,Fe)N_x	-600V	20.0	289	0.069	0.096
(Ti,Fe)N_x	-600V	15.8	256	0.062	0.06
Fe(Ti)N_x	-	14.9	239	0.062	0.058
Fe(Ti)N_x	-	14.2	245	0.058	0.048
Fe(Ti)N_x	-	13.1	233	0.056	0.041
Fe(Ti)N_x	-	14.2	233	0.061	0.053
Fe(Ti)N_x	-	14.2	246	0.058	0.047
Fe(Ti)N_x	-	17.3	271	0.064	0.071
Fe(Ti)N_x	-	19.3	283	0.068	0.090
Fe(Ti)N_x	-	19.9	281	0.071	0.100
FeN	-	15.4	259	0.059	0.054
FeN	-	9.6	229	0.042	0.017

[§] The hardness and elastic moduli quoted are for film-only values determined from the plateau (load-invariant) region of the hardness vs. depth plot and film-only elastic modulus obtained by extrapolation to zero depth according to ISO 14577-4. The film-only reduced indentation moduli have been converted to Elastic moduli using a Poisson's ratio for the films of 0.22.

Figure captions

1. High resolution SEM of nano-scratch tests on (a) FeN film with H^3/E^2 = 0.017 GPa (b) TiFeN film with H^3/E^2 = 0.090 GPa (c) TiFeN film with H^3/E^2 = 0.17 GPa (d) TiFeN film with H^3/E^2 = 0.19 GPa.

2. Variation in the L_{c2} critical load for film failure with mechanical properties (a) film hardness (b) H/E of the film (c) H^3/E^2 of the film.

3. Friction coefficient vs. load (a) TiFeN films with H^3/E^2 = 0.09-0.19 GPa (open circles) and TiN films with H^3/E^2 = 0.13-0.15 GPa (closed circles) (b) expanded view of 0-70 mN results.

4. Friction coefficient reproducibility illustrated by three repeat tests on (a) TiFeN with film H^3/E^2 = 0.13 GPa (b) TiFeN with film H^3/E^2 = 0.060 GPa.

5. Evolution of the tensile stress with (a) load and (b) hardness at 50 mN

6. The relationship between scratch toughness and H^3/E^2 of the (Ti,Fe)N_x films

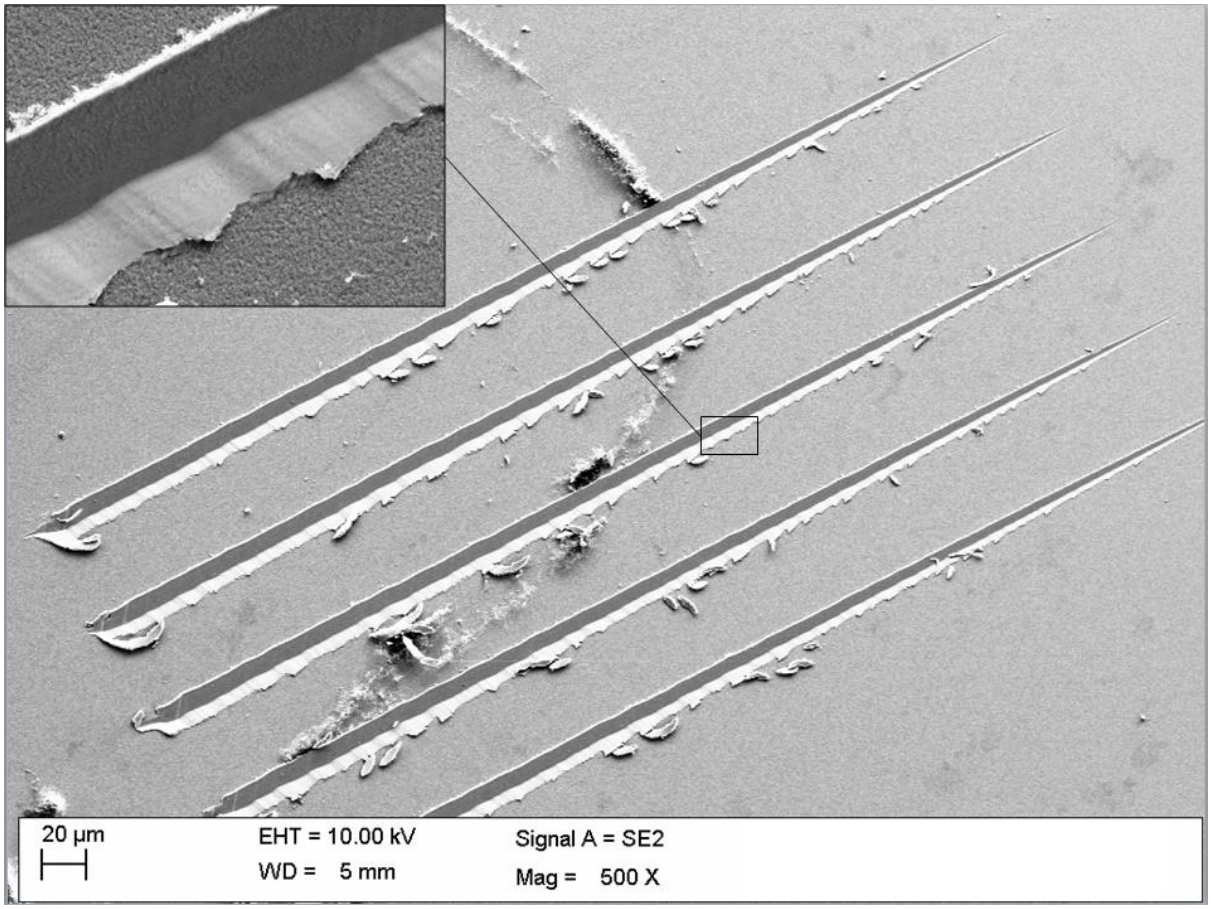

1(a)

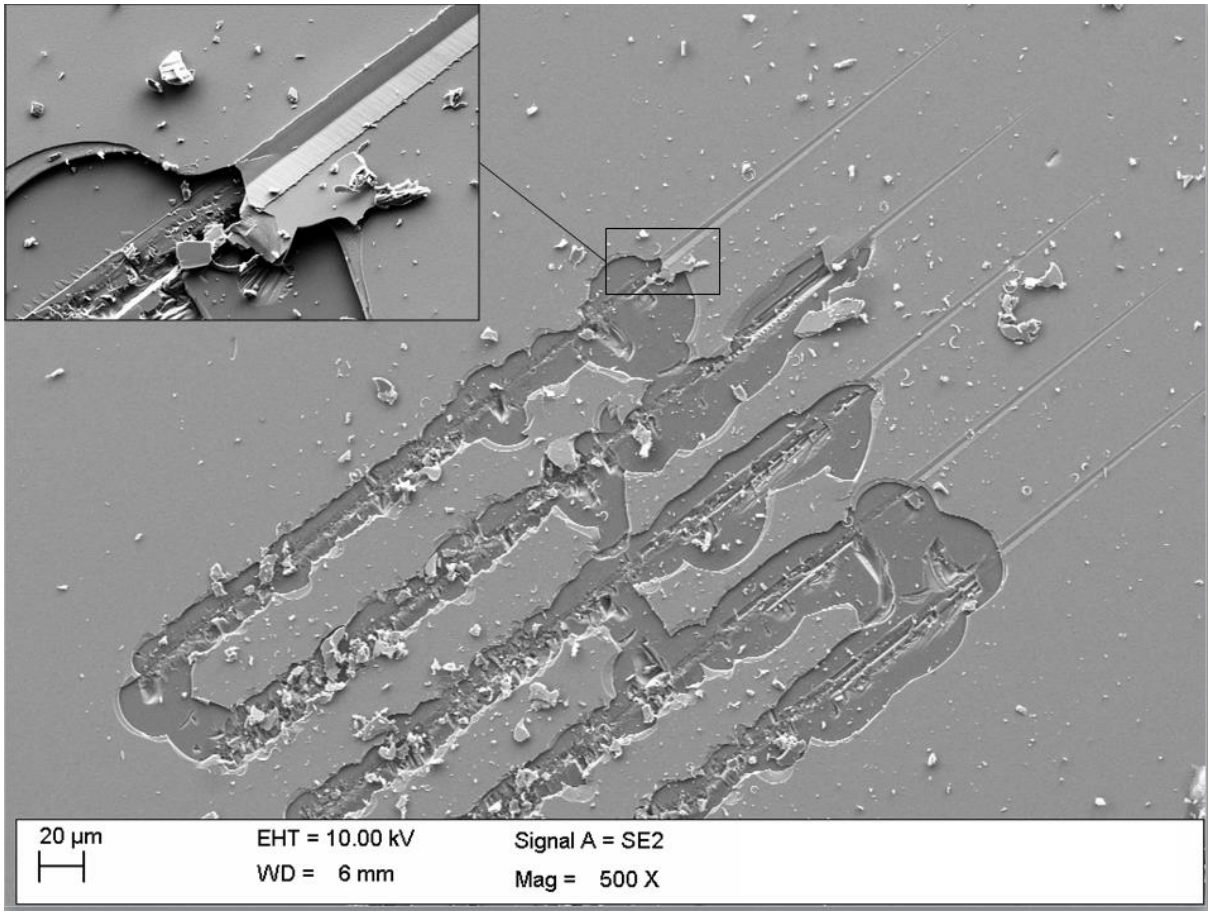

1(b)

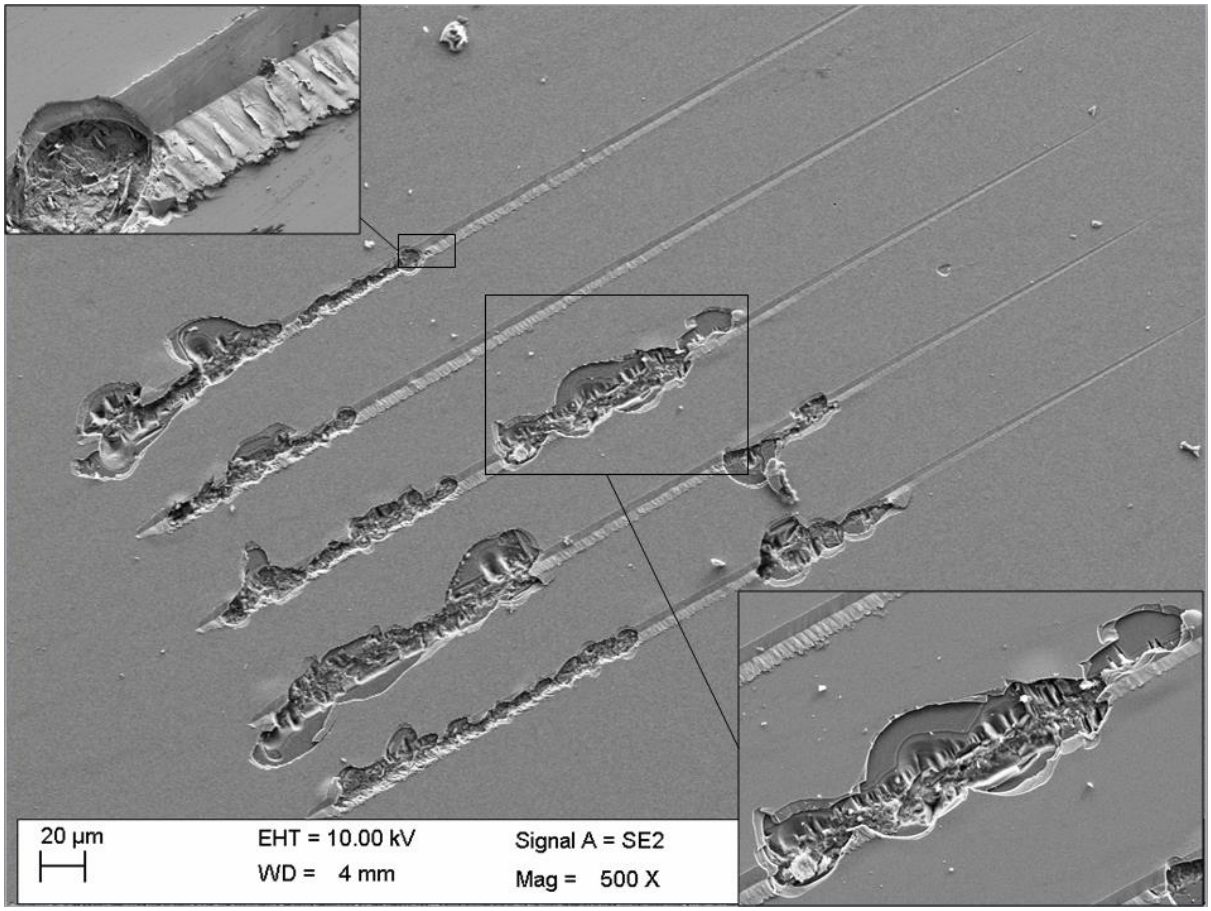

1(c)

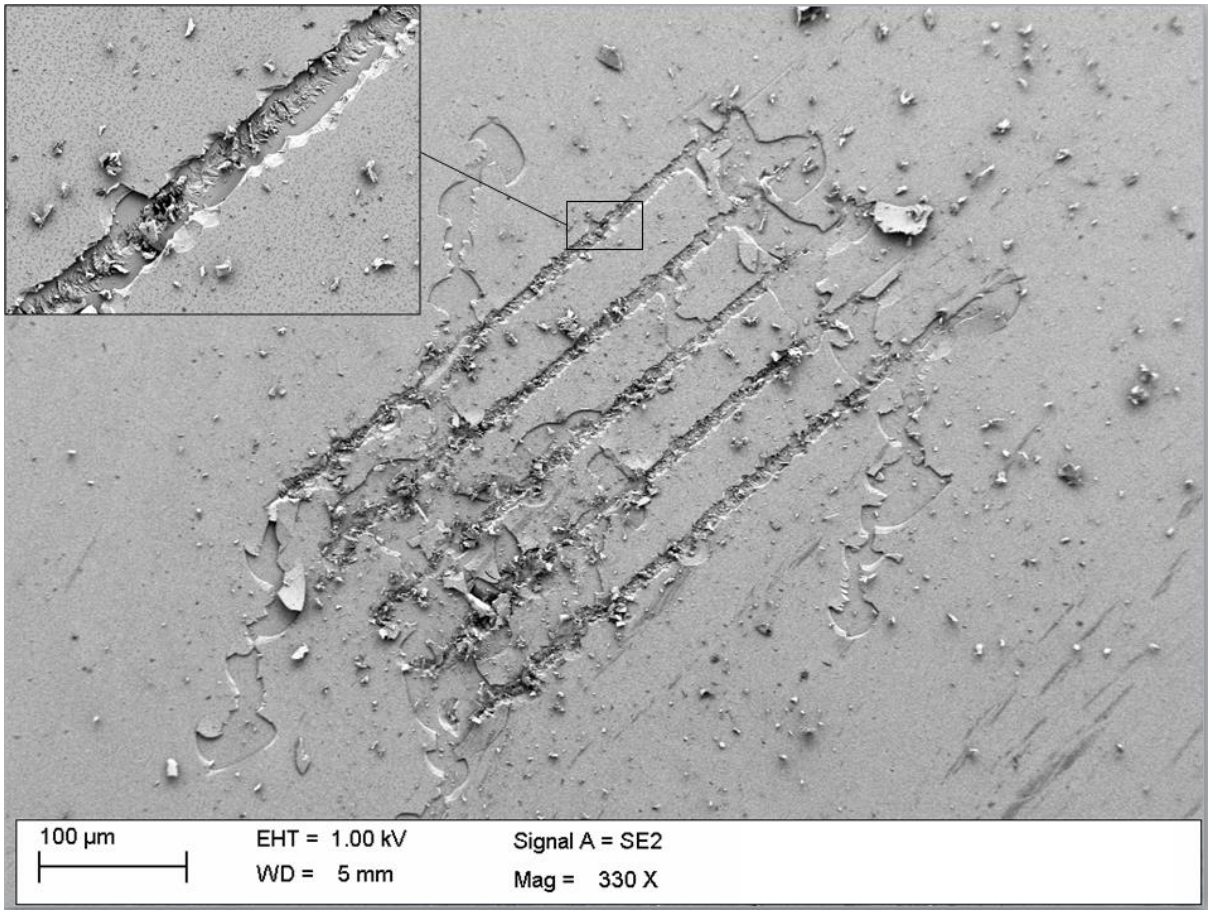
100 µm
EHT = 1.00 kV
WD = 5 mm
Signal A = SE2
Mag = 330 X

1(d)

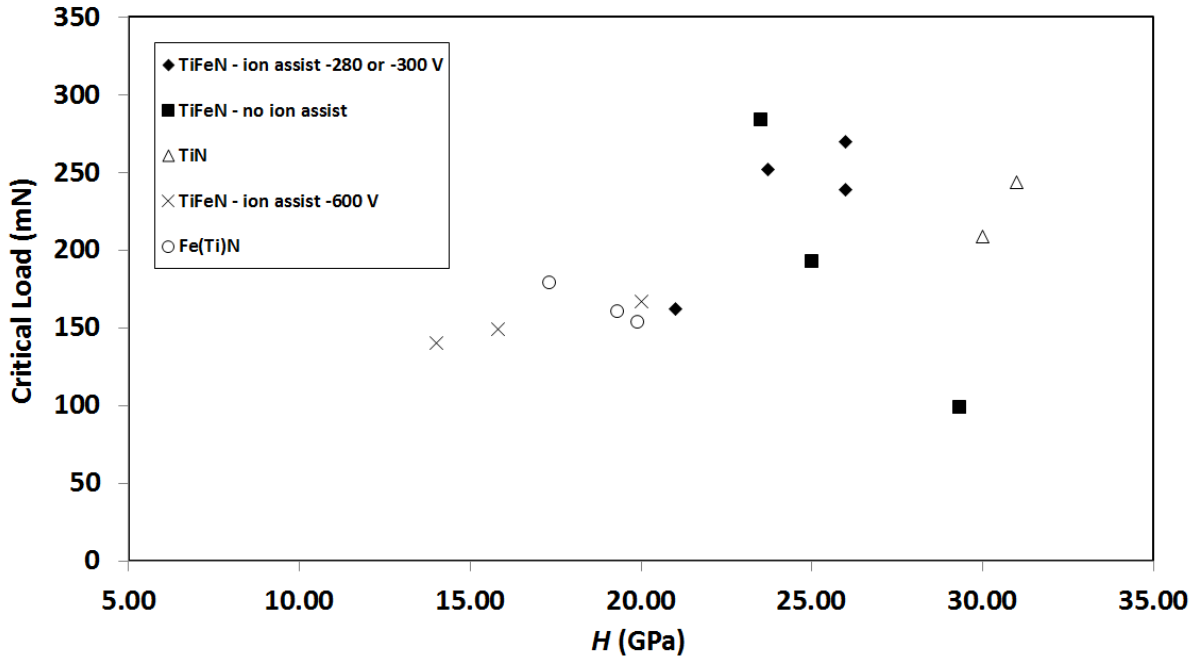
TiFeN - ion assist -280 or -300 V
TiFeN - no ion assist
TiN
TiFeN - ion assist -600 V
Fe(Ti)N
Critical Load (mN)
H (GPa)
350
300
250
200
150
100
50
0
5.00
10.00
15.00
20.00
25.00
30.00
35.00

2(a)

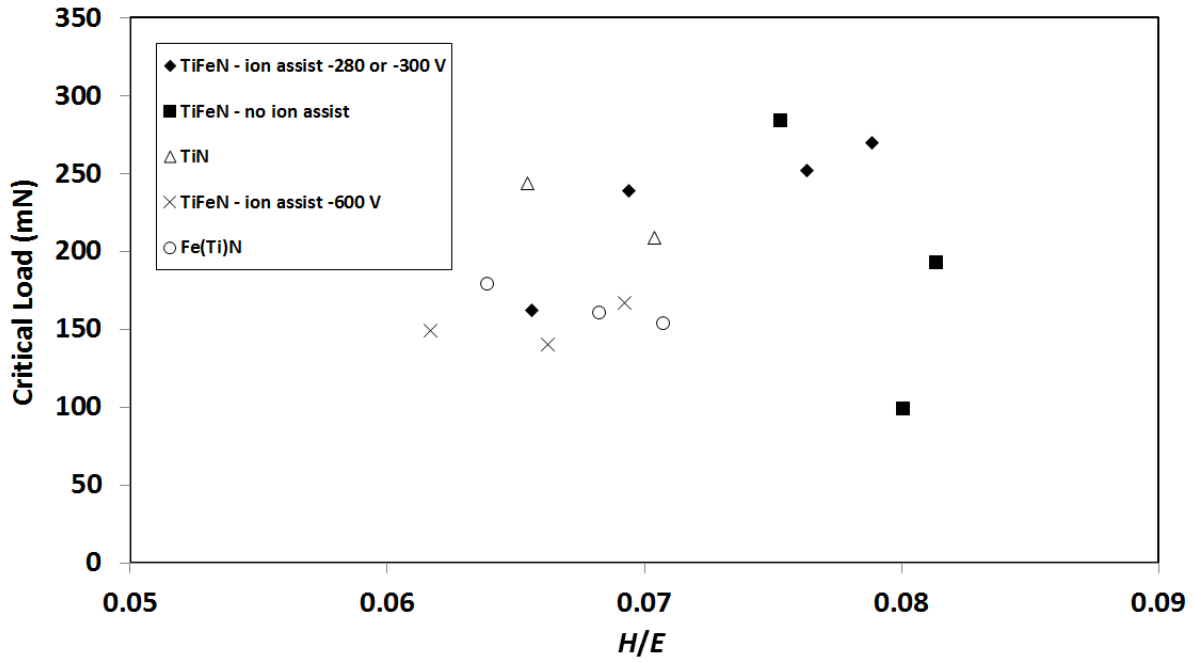
TiFeN - ion assist -280 or -300 V
TiFeN - no ion assist
TiN
TiFeN - ion assist -600 V
Fe(Ti)N
Critical Load (mN)
350
300
250
200
150
100
50
0
0.05
0.06
0.07
0.08
0.09
H/E

2(b)

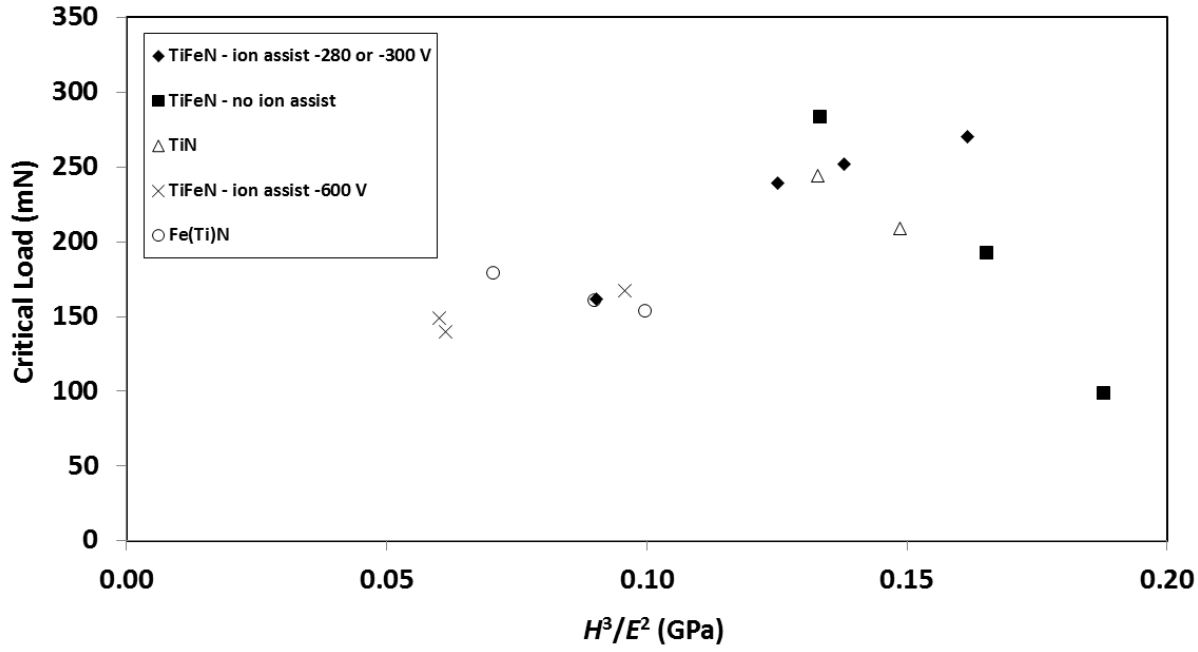
TiFeN - ion assist -280 or -300 V
TiFeN - no ion assist
TiN
TiFeN - ion assist -600 V
Fe(Ti)N
Critical Load (mN)
350
300
250
200
150
100
50
0
0.00
0.05
0.10
0.15
0.20
H3/E2 (GPa)

2(c)

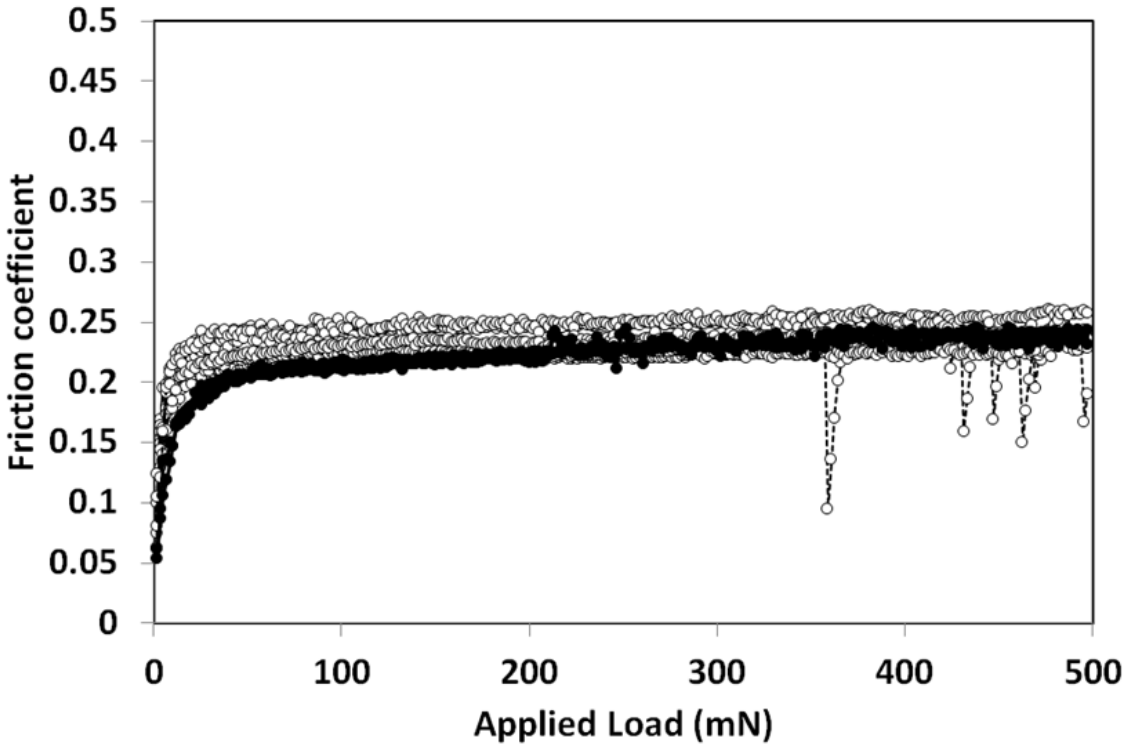
Friction coefficient
0.5
0.45
0.4
0.35
0.3
0.25
0.2
0.15
0.1
0.05
0
0
100
200
300
400
500
Applied Load (mN)

3(a)

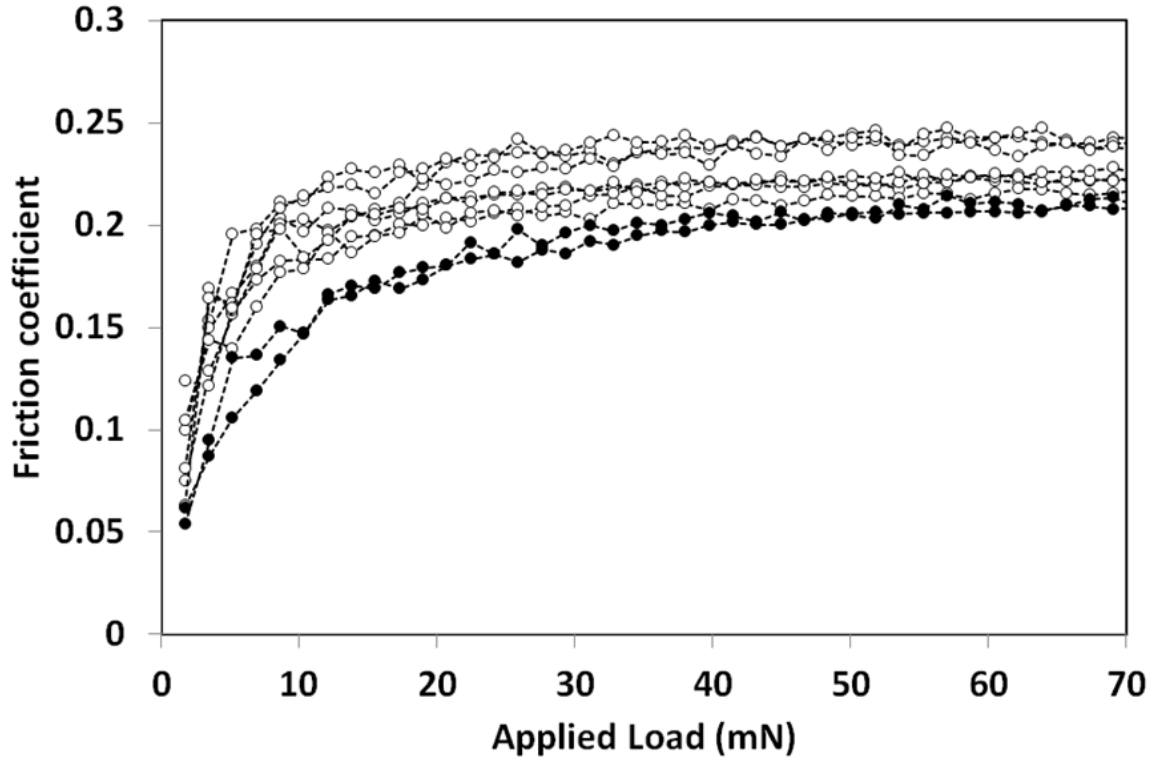
Friction coefficient
0.3
0.25
0.2
0.15
0.1
0.05
0
0
10
20
30
40
50
60
70
Applied Load (mN)

3(b)

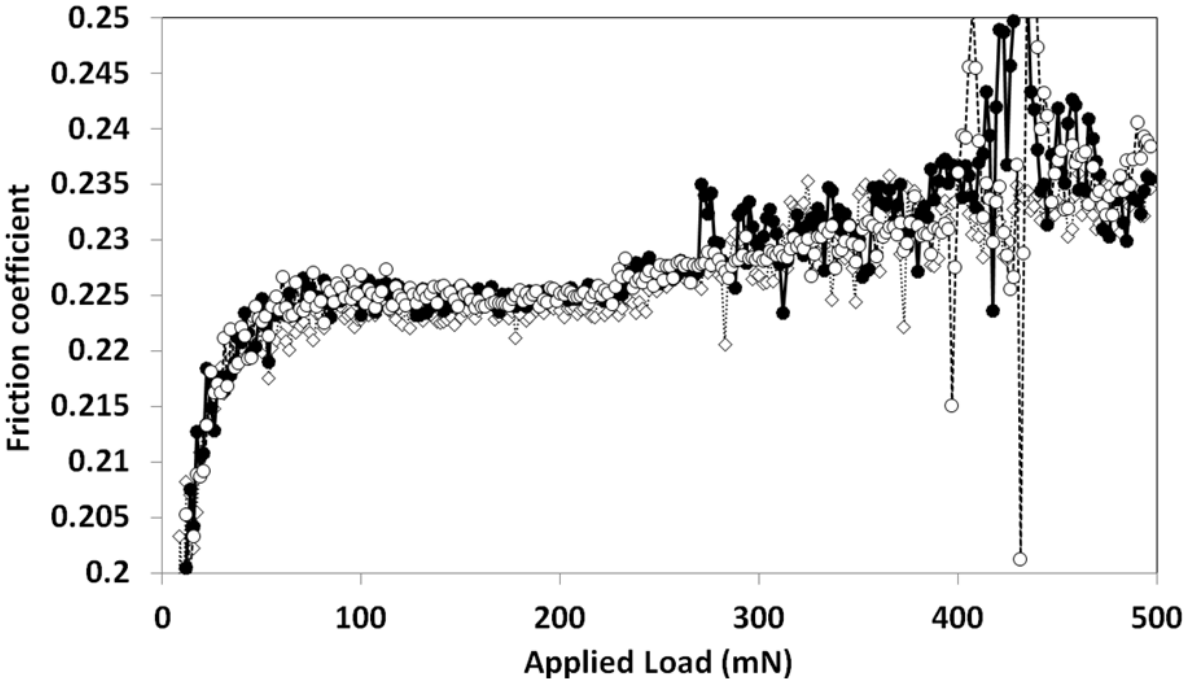
Friction coefficient
0.25
0.245
0.24
0.235
0.23
0.225
0.22
0.215
0.21
0.205
0.2
0
100
200
300
400
500
Applied Load (mN)

4 (a)

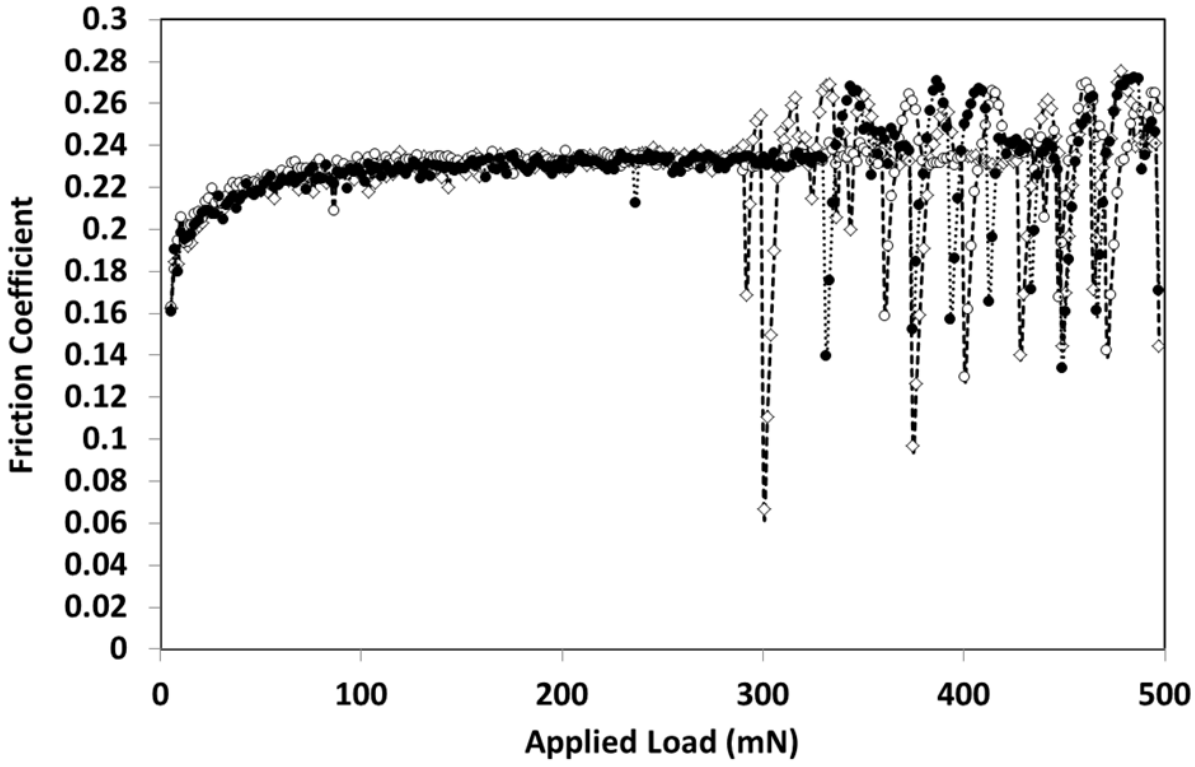
Friction Coefficient
0.3
0.28
0.26
0.24
0.22
0.2
0.18
0.16
0.14
0.12
0.1
0.08
0.06
0.04
0.02
0
0
100
200
300
400
500
Applied Load (mN)

4(b)

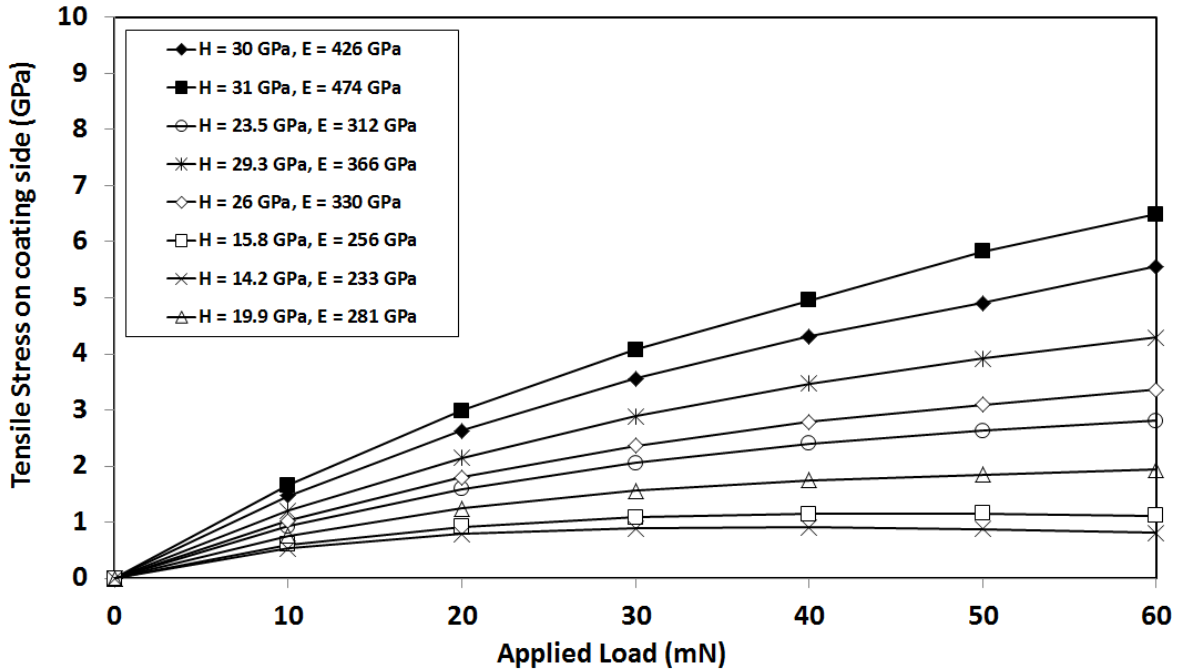
H = 30 GPa, E = 426 GPa
H = 31 GPa, E = 474 GPa
H = 23.5 GPa, E = 312 GPa
H = 29.3 GPa, E = 366 GPa
H = 26 GPa, E = 330 GPa
H = 15.8 GPa, E = 256 GPa
H = 14.2 GPa, E = 233 GPa
H = 19.9 GPa, E = 281 GPa
Tensile Stress on coating side (GPa)
Applied Load (mN)
0
1
2
3
4
5
6
7
8
9
10
0
10
20
30
40
50
60

5(a)

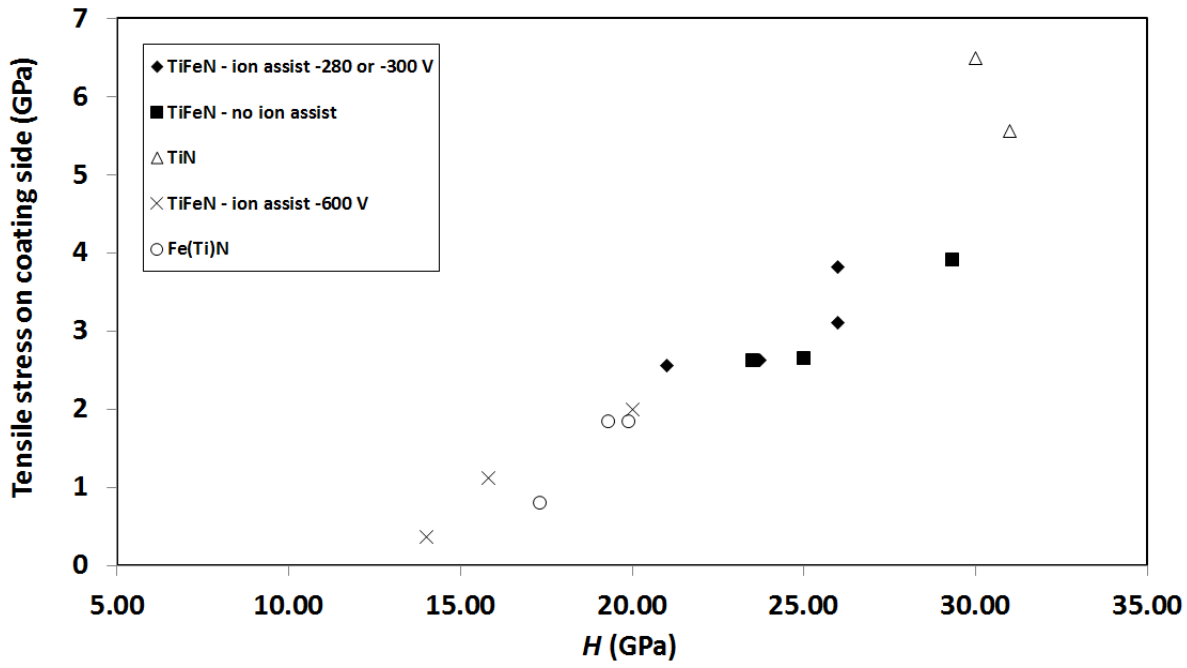
TiFeN - ion assist -280 or -300 V
TiFeN - no ion assist
TiN
TiFeN - ion assist -600 V
Fe(Ti)N
Tensile stress on coating side (GPa)
H (GPa)
0
1
2
3
4
5
6
7
5.00
10.00
15.00
20.00
25.00
30.00
35.00

5(b)

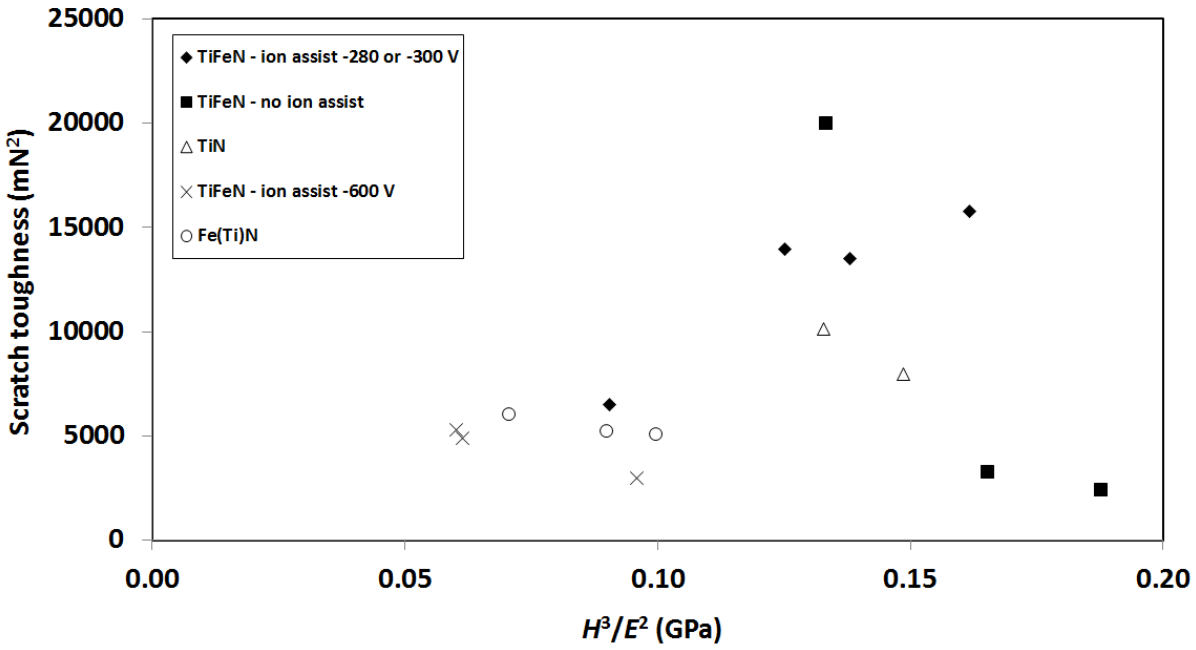
25000
20000
15000
10000
5000
0
Scratch toughness (mN²)
TiFeN - ion assist -280 or -300 V
TiFeN - no ion assist
TiN
TiFeN - ion assist -600 V
Fe(Ti)N
0.00
0.05
0.10
0.15
0.20
H³/E² (GPa)

6.